Int. J. Heat Mass Transfer. Vol. 31, No. 10, pp. 1969–1977, 1988
Printed in Great Britain

0017–9310/88 $3.00 + 0.00

Natural convection in confined fluids with combined horizontal temperature and concentration gradients

J. LEE, M. T. HYUN and K. W. KIM
Department of Mechanical Engineering, Yonsei University, Seoul 120, Korea

(*Received* 14 *September* 1987 *and in final form* 17 *February* 1988)

Abstract—Steady-state natural convection of a salt–water solution due to the combined horizontal temperature and concentration gradients is studied experimentally in rectangular enclosures of aspect ratio, 0.2 and 2.0. There appears to be two types of global fluid motion, i.e. a unicell flow pattern and a multi-layer flow pattern depending on the relative magnitude of the buoyancy ratio. Formation and growth of a layered flow structure is visually observed. A larger number of layers appear in the case of the opposing thermal and solutal buoyancy forces than that of the cooperating case. Due to the double-diffusive nature of heat and salt, interesting temperature and concentration profiles are obtained in the multi-layer flow regime.

1. INTRODUCTION

FLUID flows generated by buoyancy due to the simultaneous temperature and concentration gradients are generally referred to as 'thermosolutal convection' or 'double-diffusive convection'. It was pointed out that various modes of convection are possible depending on how both gradients are oriented relative to themselves as well as to the body force [1, 2]. Since it is related to many transport processes in nature and technology, thermosolutal convection has received much attention over the past two decades. Recently with the need for even more perfect crystals from the high technology industries, much attention is being given to the role of thermosolutal convection in crystal growth systems, which also motivated the present study. The growth of crystals is a coupled process of heat and mass transfer and it is well known that the transport process in the fluid phase during the growth of a crystal has a profound influence on the structure and quality of the solid phase.

Most of the earlier works on thermosolutal convection has been given to the situation in which both gradients are parallel to the body force direction, in order to explain some unusual oceanographic phenomena such as salt finger and salt fountains in deep sea ocean [3]. Relatively recent research has been done on natural convection in confined stratified fluids with an imposed lateral temperature gradient [4–7], but little has been done on the natural convection with combined horizontal temperature and concentration gradients which has an important bearing on the crystal growth systems. Wang *et al.* [8] initiated an experiment on this problem employing a copper sulphate–acid solution ($CuSO_4 + H_2SO_4 + H_2O$). An electrochemical system based on a diffusion-controlled electrode reaction was used to create the horizontal concentration gradient. Kamotani *et al.* [9] carried out more detailed investigations using similar experimental apparatus. They found a three-layered flow structure in the core for the larger buoyancy ratio independent of the direction of temperature and concentration gradients, and a unicell flow pattern for the lower buoyancy ratio. Under certain conditions, a secondary cell appears in the unicell flow pattern near the electrodes and the flow in the solutal boundary layer fluctuates randomly. Both works, however, were not performed under steady-state conditions, because the horizontal concentration gradient varied during the experiment due to the thermal convection and electrolysis. This, presumably, is the main source of the difficulties delaying the experimental study on this type of problem. In the present work, an experiment is performed to study steady-state natural convection of a salt–water solution in rectangular enclosures of aspect ratio, 0.2 and 2.0, with the combined horizontal temperature and concentration gradients. The primary objective is to obtain the basic information of the natural convection flow pattern with the corresponding temperature and concentration distributions under various parametric conditions. Measurement and flow visualization show complex, but interesting flow phenomena.

2. EXPERIMENTS

2.1. *Experimental apparatus*

A schematic diagram of the experimental set-up for $Ar = 0.2$ is given in Fig. 1. The test section is a horizontally placed rectangular enclosure 30 mm high, 150 mm wide and 170 mm deep for $Ar = 0.2$, and 60 mm high, 30 mm wide and 120 mm deep for $Ar = 2.0$, respectively. Each end wall of the test section consists of a membrane with supply reservoirs, which is

NOMENCLATURE

Ar	aspect ratio, H/L	Sc	Schmidt number, ν/D
ΔC	concentration difference [wt.%]	ΔT	temperature difference [°C]
D	diffusivity of salt [$m^2 s^{-1}$]	x	horizontal coordinate [m]
g	acceleration due to gravity [$m s^{-2}$]	y	vertical coordinate [m].
H	height of the enclosure [m]		
L	width of the enclosure [m]	Greek symbols	
Le	Lewis number, α/D	α	thermal diffusivity [$m^2 s^{-1}$]
N	buoyancy ratio, $(\bar{\beta}\Delta C)/(\beta\Delta T)$	β	thermal expansion coefficient [$°C^{-1}$]
Pr	Prandtl number, ν/α	$\bar{\beta}$	solutal expansion coefficient [wt.%$^{-1}$]
Ra_S	solutal Rayleigh number, $(g\bar{\beta}\Delta C H^3)/(\nu\alpha)$	δ_S	solutal boundary layer thickness [m]
Ra_T	thermal Rayleigh number, $(g\beta\Delta T H^3)/(\nu\alpha)$	δ_T	thermal boundary layer thickness [m]
		ν	kinematic viscosity [$m^2 s^{-1}$].

worked out to impose the constant lateral temperature and concentration gradients across the enclosure. Many different types of membranes were tried in the experiment and the cellulose acetate type membrane for dialysis was found to work best. The shortcoming of using a cellulose acetate membrane is that it cannot stand the high temperature (>50°C), thus the parametric ranges are somewhat limited. In addition, the osmosis process may seem to be influenced by the fluid flow near the boundaries. But, considering that the osmosis process is very fast in the salt–water solution due to the very high osmotic pressure and that the flow is very slow within a solutal boundary layer at the end wall, the effect does not seem to be appreciable. The membrane adopted in the present test is 250 PM type made by Enca Company in Germany. The whole set-up except the vertical end wall is made of 10 mm thick acryl plate and is enclosed by styrofoam 30 mm thick to minimize the heat loss from the system to the surroundings.

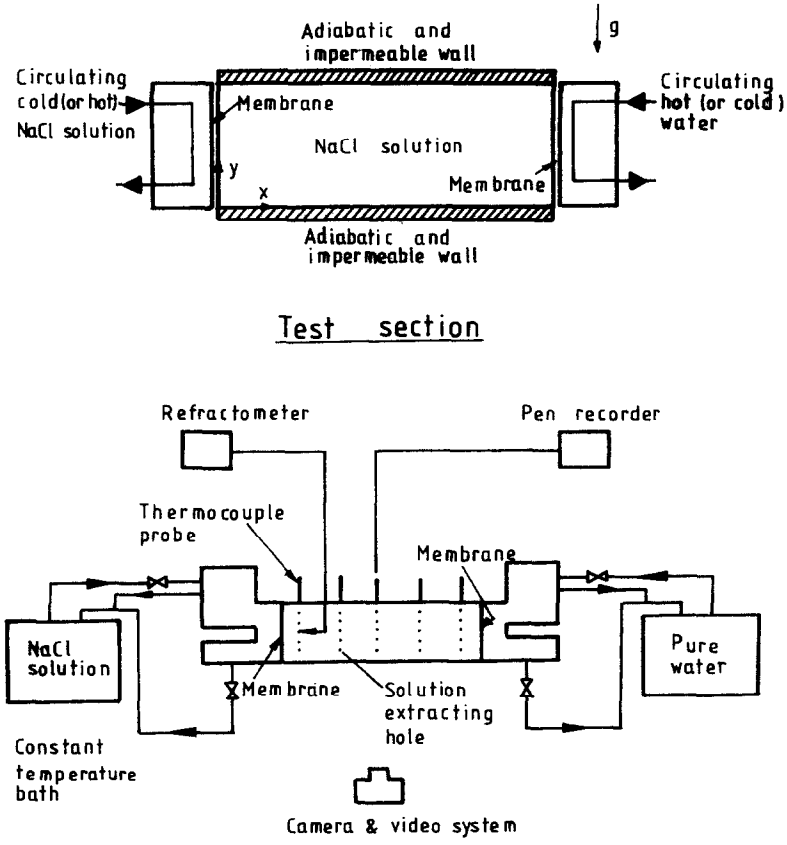

FIG. 1. Schematic diagram of the experimental set-up for $Ar = 0.2$.

Pure water and a salt–water solution are used as the working fluids. Each solution adjusted to the experimental conditions circulates through the supply reservoir from the two constant temperature baths. The flow rate to and from the reservoir is controlled by the flow valve. Thermocouples are imbedded in each of the inflow and outflow sections of the reservoirs to determine the temperature of the supplying solutions. The traversing probes made of copper–constantan thermocouples are inserted into the test section for temperature measurement through 1.5 mm o.d. holes in the upper plate. A multi-pen recorder is occupied to record all thermocouple data. In order to determine the concentration profiles in the test section, the electroconductivity probe was constructed using platinum wire, because point electroconductivity is generally chosen as the method of measuring the salt concentration at points in a confined enclosure [10]. We found, however, that the calibration is changed due to the increasing probe resistance during the measurement. Both gain and reference, thus, had to be adjusted between calibrations in order to make the second calibration meaningful. Therefore, the sample extraction method is used here instead, and for this purpose holes of 1 mm diameter are made in the back side of the wall. Through the hole a minute amount of solution is extracted by fine needles of 0.3 mm i.d. and its refractive indexes are read through the Abbe refractometer.

2.2. *Test procedure*

The thermal and solutal convection are started simultaneously in the experiment by continuously circulating pure water kept at a given temperature in the right end wall and the salt–water solution maintained at constant, but different temperature and concentration in the left wall. The enclosure is initially filled with salt–water solution where the concentration is half the circulating solution in order to equalize the concentration differences at each membrane. This gives the same osmotic pressure at each end wall because it is proportional to the concentration difference. Due to osmosis phenomena at each end wall, the density near pure water (salt–water solution) becomes lower (higher) than that of the bulk solution, and solutal convection is initiated and sustained in this way interacting with the imposed thermal buoyancy due to the temperature differences.

Two types of tests have been conducted. In the first case the temperature of the high concentration wall is kept lower than that of the low concentration wall so that the thermal and solutal buoyancy are in augmentation (cooperating case). In the second case the temperature of the high concentration wall is higher than that of the low concentration wall so that two buoyancy forces are in retardation (opposing case). It takes about 10–12 h to reach the steady state for $Ar = 0.2$ and 5–6 h for $Ar = 2.0$. The temperature and concentration profiles are checked at some intervals from start up to the steady state. Temperature distributions in the test section are measured at $x/L = 1/10, 3/10, 5/10, 7/10, 9/10$ at each 2 mm depth in the vertical direction for $Ar = 0.2$ and at $x/L = 1/6, 3/6, 5/6$ at each 3 mm depth for $Ar = 2.0$. The concentration profiles are examined at 5 mm depth in the vertical direction at the same position of the temperature measurement. This procedure is repeated and each refractive index is averaged. The averaged refractive index is then converted into the concentration by a conversion chart. The deviations from the average values are within 5%. Flow patterns in the enclosure are examined by visualizing them with dye injection through the hole at the centre of the top wall or at the back wall using a camera and video-system.

The experiment covers the ranges of $Ar = 0.2$–2.0, $Pr = 4.0$–7.9, $Sc = 402$–789, $Ra_T = 1.92 \times 10^6$–2.85×10^8 ($\Delta T = 3.4$–35.9°C), $Ra_S = 6.28 \times 10^7$–2.34×10^9 ($\Delta C = 5$–20 wt.%) and $N = 2.7$–72.3. All fluid properties [11] are evaluated at the average value of both temperature and concentration of each end wall.

3. RESULTS AND DISCUSSION

In the present experiment, a solutal boundary layer type flow is always observed due to the concentration difference moving along the cavity walls confined to narrow regions. It flows from the low to high concentration end wall via the top and bottom walls independent of the direction of the imposed temperature gradient. According to Wang *et al.*'s expression [8], the ratio of end wall thermal and solutal boundary layer thicknesses for $Pr > 1$ and $Sc > 1$ is given as $\delta_T/\delta_S = (Le\,N)^{0.25}$. In this experiment $Pr = 7.5$ and $Sc = 751$ and the buoyancy ratio is in the range of 2.7–72.3 so that the thermal boundary layer is about 4–9 times thicker than the solutal boundary layer. This is not verified here because of the difficulty of measuring the concentration distributions in a very thin region near the boundaries. In each test solutal buoyancy flow is counterclockwise since the high concentration wall is on the left-hand side whereas the direction of the thermally driven flow depends on the direction of the imposed lateral temperature gradient. In the cooperating case the thermal buoyancy flow circulates in the same direction as the solutal buoyancy flow, but it circulates opposite to the solutal buoyancy flow in the opposing case. There, however, is not any evidence of shear instability between the two buoyancy flows. Flow visualization shows two types of global fluid motion in the enclosure according to the interaction of the horizontal temperature and concentration gradients; a unicell flow pattern and a multi-layer flow pattern. For $Ar = 2.0$, global fluid motion mostly appears as a multi-layer flow pattern in the present experimental range. For $Ar = 0.2$, however, there exists a definite range of Ra_T and Ra_S (i.e. buoyancy ratio) over which the multi-layer flow pattern appears. In the case of relatively larger Ra_T and smaller Ra_S (lower buoyancy ratio) there exists a fast-moving unicell flow due to the strong thermal

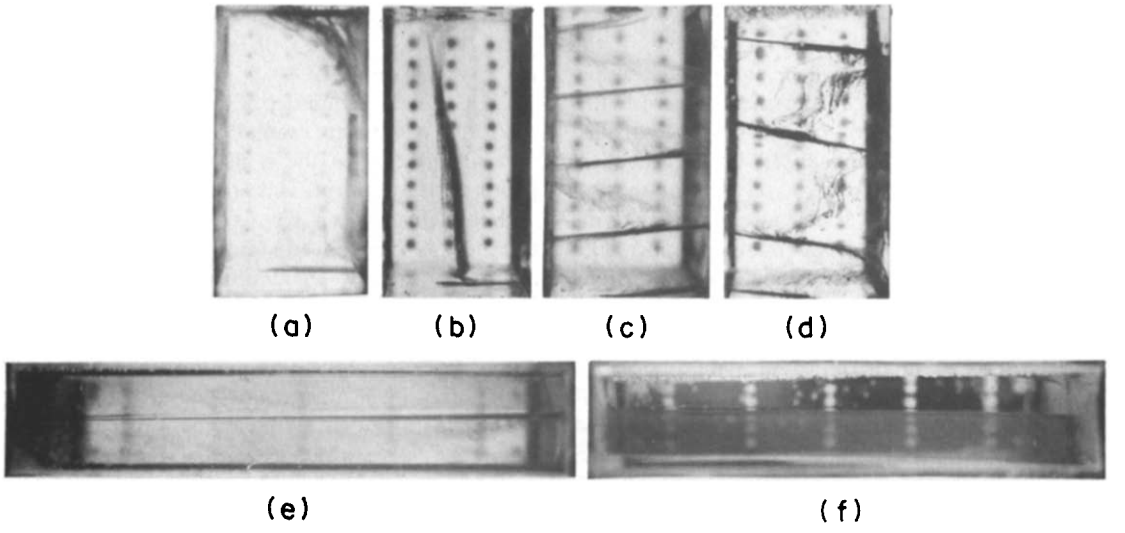

FIG. 2. Typical flow patterns in the enclosure: (a) $Ra_T = 1.05 \times 10^8$, $Ra_S = 6.02 \times 10^8$, $Ar = 2.0$ (cooperating case); (b) $Ra_T = 2.72 \times 10^7$, $Ra_S = 1.93 \times 10^9$, $Ar = 2.0$ (opposing case); (c) $Ra_T = 6.04 \times 10^7$, $Ra_S = 1.09 \times 10^9$, $Ar = 2.0$ (cooperating case); (d) $Ra_T = 2.01 \times 10^8$, $Ra_S = 1.30 \times 10^9$, $Ar = 2.0$ (opposing case); (e) $Ra_T = 1.59 \times 10^7$, $Ra_S = 1.42 \times 10^8$, $Ar = 0.2$ (cooperating case); (f) $Ra_T = 2.82 \times 10^7$, $Ra_S = 1.52 \times 10^8$, $Ar = 0.2$ (opposing case).

buoyancy imposed on the slowly-moving solutal buoyancy flow, while there appears a thin, slowly-moving unicell flow for relatively smaller Ra_T and larger Ra_S (higher buoyancy ratio) due to the strong solutal buoyancy effect. The typical flow patterns visually observed are illustrated in Fig. 2. Figures (2(a) and (b) show the unicell flow pattern each due to strong thermal and solutal buoyancy while Figs. 2(c) and (d) show multi-layer flow pattern for comparable thermal and solutal buoyancy effects for $Ar = 2.0$. Figures 2(e) and (f) show multi-layer flow pattern for $Ar = 0.2$.

Figure 3 shows a sketch of the typical formation of global flow structure with time for $Ar = 2.0$ in the enclosure. Both the cooperating and opposing cases show similar trends. The global flow structure initially appears as a fast-moving unicell flow driven by thermal buoyancy. As time progresses, however, the layers are formed near the horizontal boundaries as salt is stratified there due to the solutal buoyancy flow. They grow and become thicker to some extent as salt stratification proceeds. When the layer thickness becomes sufficiently large, the top and bottom layers detach from the wall and move into the mid-region while the new layer grows again at the boundaries. Layers are formed successively in this manner until the steady state is reached. The thickness of each layer is the same except for the top and bottom layers. In the opposing case, it is sometimes observed that a new layer is formed at the interface of the mid-core. Kamotani *et al.* [9] explained that the layered flow pattern is produced due to the density change caused by the extraction of solution from the solutal boundary layer by the thermally driven flow. In the present experiment, by a careful measurement and flow observation, the mechanism of layer formation is supposed to be as follows. When the test is run, the lighter (heavier) fluid in the solutal boundary layer moves up (down) along the end wall and accumulates for a long time near the top (bottom) wall due to the very slow movement there (this, of course, is influenced by the thermally driven flow). Salt stratification occurs in the region near the horizontal boundaries and extends with time due to the diffusion of salt between the bulk solution and the horizontal solutal layer. When the solutal stratification near the top and bottom wall is sufficient enough to balance local thermal buoyancy there, there appears a layered-flow structure and the global flow pattern changes. The multi-layer flow patterns obtained are very similar to those occurring in Thorpe *et al.*'s work [4] where an initially vertically stratified fluid is subjected to a horizontal temperature gradient. The difference is that in their experiment the layers are simultaneously formed throughout the enclosure while in the present work the layers are successively formed from the top and bottom walls. The first layered-flow structure for $Ar = 2.0$ appears at about 15 min after the experiment is started and it appears at about 30 min for $Ar = 0.2$. When the thermal buoyancy effect is dominant over the solutal buoyancy effect (lower buoyancy ratio), global fluid motion turns up as a strong unicell flow pattern from the beginning until the steady state is reached. In this case, thermal convection is strong enough to prevent the solution from stratifying at the boundaries and, as a result, the layered-flow structure is not found at any time. When the solutal buoyancy effect is dominant (higher buoyancy ratio), the steady-state global flow pattern is also unicell flow, but the formation of the flow structure is quite different from that of the strong thermal buoyancy case. Because heat diffuses

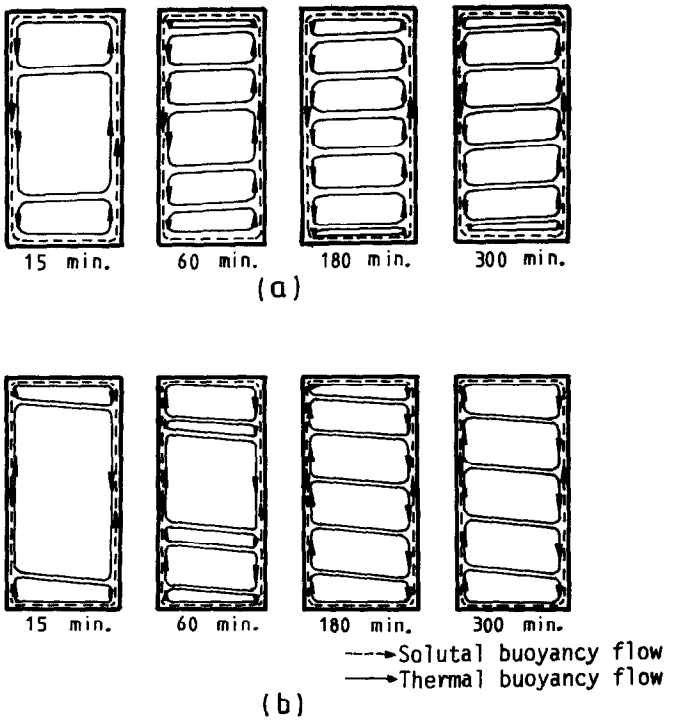

FIG. 3. Formation of layered-flow structure with time for $Ar = 2.0$: (a) $Ra_T = 2.69 \times 10^7$, $Ra_S = 1.10 \times 10^9$ (cooperating case); (b) $Ra_T = 6.31 \times 10^7$, $Ra_S = 6.12 \times 10^8$ (opposing case).

far faster than salt, global fluid motion initially appears as a slowly-moving unicell flow driven by the weak thermal buoyancy. As time progresses, however, there appears a layered flow adjacent to the top and bottom walls where solute is stratified and the global flow pattern changes into a three-layered flow structure. Since thermal buoyancy is too small to bring up and move the solute, the diffusion of salt either to or from the middle layer takes place at the interfaces of each layer. The stratification thus continues and extends into the mid-core region with time from the top and bottom walls while the top and bottom layers grow and become thicker. Finally the interfaces separating the top and bottom layers from the middle layer disappears and the thermally driven flow is no longer observed. This is obviously due to the strong retardation effect of solutal stratification over the weak thermal buoyancy effect. This is more clearly seen under the circumstances of the opposing case where the solutal buoyancy flow is in the opposite direction to the thermal buoyancy flow. The global flow remains as a solutally-driven unicell flow circulating counterclockwise along the cavity and fluid motion in the core region is nearly stagnant.

The steady-state temperature and concentration profiles at $x/L = 1/10$, $5/10$, $9/10$ for $Ar = 0.2$ and $x/L = 1/6$, $3/6$, $5/6$ for $Ar = 2.0$ are given in Figs. 4–6. The fact that the value of concentration is lowest at the top and highest at the bottom of the enclosure as shown in Figs. 4–6 clearly indicates the existence of solutal buoyancy flow visually observed. Data points near the top and bottom walls in the concentration profiles are connected with a dotted line due to the uncertainty of the concentration variations in those regions, because we did not measure the local value of salinity there. Figure 4(a) shows the case of the lower buoyancy ratio for $Ar = 2.0$, in which the global flow structure appears as a fast-moving unicell flow. Corresponding temperature profiles in the core are almost linearly stratified except in the region near the horizontal boundaries, which is similar to those observed in the case of pure thermal convection [12]. Concentration is uniformly distributed in the core except the thin layer near the horizontal boundaries because the diffusion of salt from and into the core is negligible and salinity is well mixed in the core by the strong thermal buoyancy flow. Figure 4(b) is the case of the higher buoyancy ratio for $Ar = 2.0$, where a thin, slowly-moving unicell flow appears resulting from the strong solutal buoyancy effect. The core temperature profiles are almost linear in the horizontal direction with a small variation in the vertical direction, implying that conduction is the dominant mode of heat transfer in this case. The core concentration distributions are vertically stratified with a small variation in the horizontal direction.

Figures 5 and 6 show the vertical temperature and concentration profiles of the multi-layer flow appearing in the intermediate buoyancy ratio for $Ar = 0.2$ and 2.0, respectively. Each layer circulates from the hot to the cold end wall and slightly slopes downward as it approaches the cold end wall, because the density

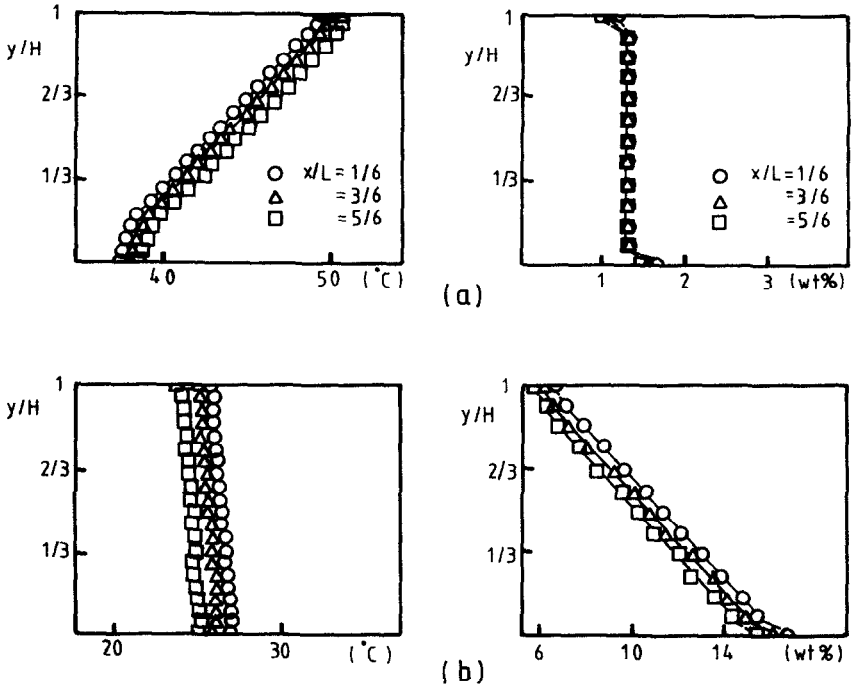

FIG. 4. Vertical temperature and concentration profiles in the case of unicell flow for $Ar = 2.0$: (a) $Ra_T = 2.06 \times 10^8$, $Ra_S = 7.44 \times 10^8$ (cooperating case); (b) $Ra_T = 2.48 \times 10^7$, $Ra_S = 1.08 \times 10^9$ (opposing case).

increases due to the cooling effect of the end wall. The number of layers appearing in the enclosure depends on the imposed direction and the relative magnitude of both gradients in each case. The velocity of each layer is different. The layer in the mid-core is faster than that at the top and bottom walls. The temperature variation in each layer largely depends on the layer velocity. Temperature varies both hori-

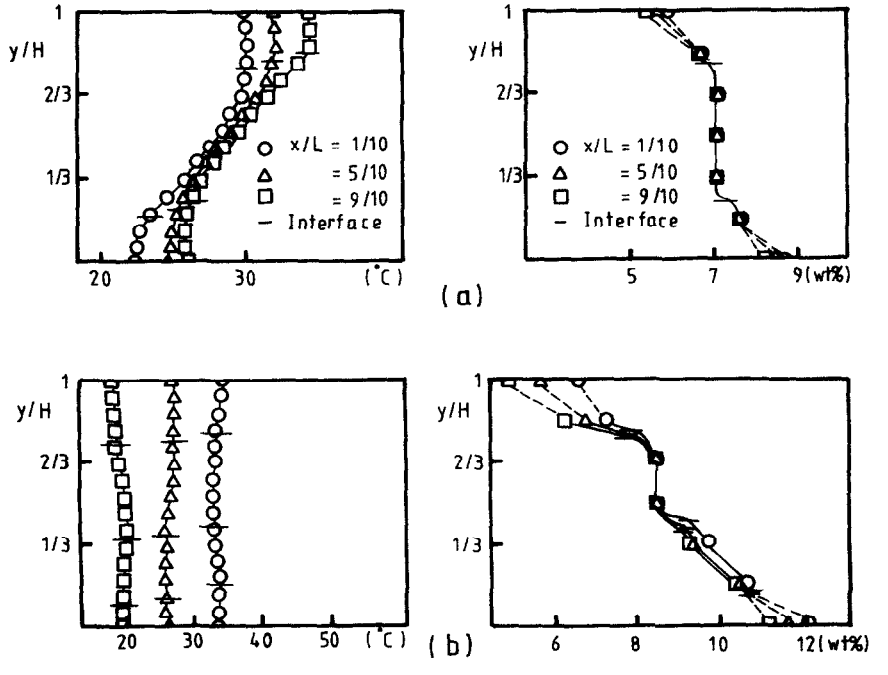

FIG. 5. Vertical temperature and concentration profiles in the case of multi-layer flow for $Ar = 0.2$: (a) $Ra_T = 1.62 \times 10^7$, $Ra_S = 2.01 \times 10^8$ (cooperating case); (b) $Ra_T = 1.85 \times 10^7$, $Ra_S = 1.96 \times 10^8$ (opposing case).

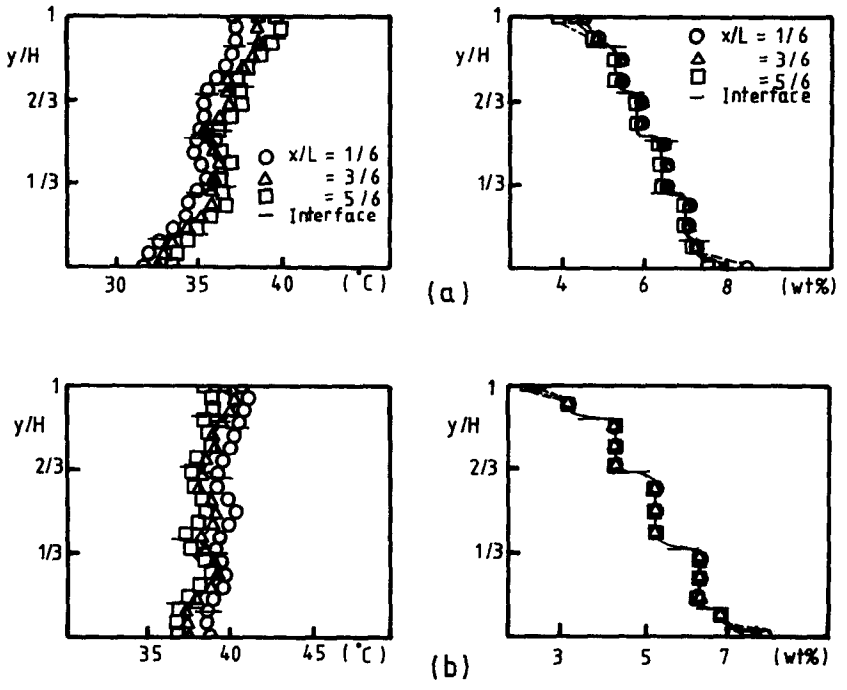

FIG. 6. Vertical temperature and concentration profiles in the case of multi-layer flow for $Ar = 2.0$: (a) $Ra_T = 9.43 \times 10^7$, $Ra_S = 1.78 \times 10^9$ (cooperating case); (b) $Ra_T = 2.85 \times 10^8$, $Ra_S = 1.42 \times 10^9$ (opposing case).

zontally and vertically in the fast-moving layer (the middle layer of Figs. 5(a) and 6) while it mostly changes in the horizontal direction in the slowly-moving layer such as the top and bottom layers of Figs. 5 and 6. As the fast-moving layer becomes thicker and faster in the mid-core, the temperature change in the horizontal direction diminishes and its profiles get closer to that of pure thermal convection, implying that the thermal convection by the fast-moving layer is appreciable. For $Ar = 2.0$, the velocity of the layers in the mid-core is nearly equal so that the temperature profiles of each layer are of the same form. This trend is similar in the opposing case. But in the opposing case of $Ar = 0.2$, the temperature variation does not differ much between the fast-moving layer (the upper middle layer in Fig. 5(b)) and the slowly-moving layer (the other layers in Fig. 5(b)). In this case, the temperature varies rather appreciably in the horizontal direction than in the vertical direction, thus convection does not seem to be appreciable in each layer. Conduction should be the dominant mode of heat transfer. The concentration profiles show a similar trend in both the cooperating and opposing cases according to the layer velocity. Concentration distributes uniformly in the fast-moving layer while it is stably stratified in the slowly-moving layer except near the top and bottom walls where a small horizontal variation exists. Temperature varies smoothly at the interface of each layer, but concentration varies rapidly at the interface neighbouring the fast-moving layer (Figs. 5(a) and 6) whereas it changes smoothly at the

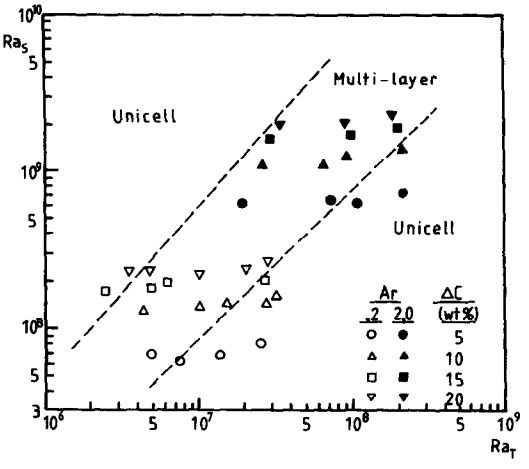

FIG. 7. Flow patterns depending on thermal and solutal Rayleigh numbers in the cooperating case.

interface of the slowly-moving layer (Fig. 5(b)). This phenomena is largely due to the difference of the diffusivities of heat and salt ($Le \simeq 100$). Heat with larger diffusivity diffuses at the interface fast enough to have smooth temperature variations even in the case of a fast-moving layer, but salt with much lower diffusivity cannot diffuse so rapidly as to have the smooth concentration variations at the interface when the layer velocity is large.

Unicell and multi-layer flow regimes are represented in Figs. 7 and 8 for the cooperating and opposing cases, respectively. Though the demarcation

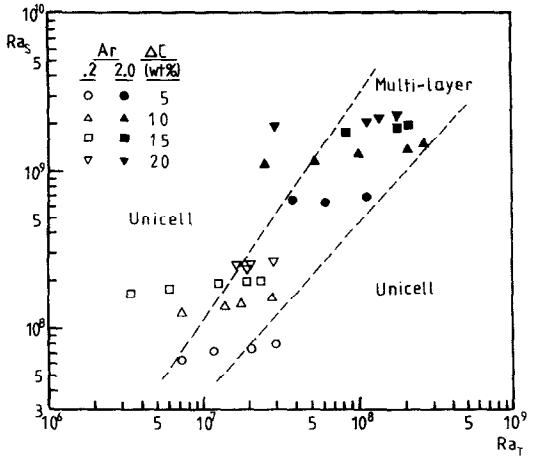

FIG. 8. Flow patterns depending on thermal and solutal Rayleigh numbers in the opposing case.

is not applicable with confidence for $Ar = 2.0$, it is generally admitted for $Ar = 0.2$ that there is a certain range of Ra_T for a given Ra_S or vice versa (i.e. buoyancy ratio) over which the multi-layer flow structure appears. As mentioned above, the unicell flow pattern appears for relatively larger Ra_T and smaller Ra_S (lower buoyancy ratio) and vice versa (higher buoyancy ratio), while the multi-layer flow pattern appears over the intermediate ranges of Ra_T and Ra_S. In the present experiments multi-layer flow patterns for $Ar = 0.2$ are observed when the buoyancy ratio is in the range of 8–55 for the cooperating case and 5–13 for the opposing case. At one view, this seems to be in contrast to Kamotani *et al.*'s observation [9]. They found only a three-layered flow structure for a relatively large buoyancy ratio and a unicell flow pattern for decreasing buoyancy ratio. But, considering that their experimental ranges lie in the lower right portion of Figs. 7 and 8, it could be expected that there appears a unicell flow due to the strong solutal buoyancy if the experimental ranges are extended to much higher buoyancy ratio. The multi-layer flow region is much narrower in width and lies more to the right in the opposing case, implying that the multi-layer flow appears at a larger Ra_T for about the same Ra_S. The number of layers in both cases increase for the increasing buoyancy ratio in a multi-layer flow regime and more layers appear in the opposing case than in the cooperating case at about the same parametric conditions.

4. SUMMARY

This paper presents the result of an experimental study of natural convection due to the combined horizontal temperature and concentration gradients in rectangular enclosures of aspect ratio, 0.2 and 2.0. Global fluid motion in the enclosure appears as a unicell flow pattern for the lower and higher buoyancy ratio, while it appears as a multi-layer flow pattern for the intermediate ranges of buoyancy ratio. In addition, there always exists a solutal buoyancy flow resulting from the lateral concentration gradient, which circulates in a thin layer along the cavity walls independent of the direction of the imposed temperature gradient. In the multi-layer flow regime, the number of layers increase for increasing buoyancy ratio and more layers appear in the opposing case than that in the cooperating case. The layered flow structure does not form simultaneously, but rather grows from the top and bottom walls.

Interesting core temperature and concentration profiles are obtained according to the flow pattern. For the lower buoyancy ratio (unicell flow due to the strong thermal buoyancy), the temperature in the core is stratified except in the region near the top and bottom walls similar to those of pure thermal convection and concentration is uniformly distributed in the core. For the higher buoyancy ratio (unicell flow due to the strong solutal buoyancy), temperature varies linearly in the horizontal direction with small vertical variation and concentration is stably stratified in the core. For the intermediate buoyancy ratio (multi-layer flow regime), temperature largely varies vertically and the concentration distribution is nearly uniform in the fast moving layer, while in the slowly-moving layer the temperature largely varies horizontally and concentration is stably stratified. Due to the double-diffusive phenomena, temperature varies smoothly at the interface of each layer, but concentration varies rapidly at the interface neighbouring the fast-moving layer while it varies smoothly at the interface of the slowly-moving layers.

REFERENCES

1. J. S. Turner and H. Stommel, A new case of convection in the presence of combined vertical salinity and temperature gradients, *Proc. Natn. Acad. Sci.* **52**, 49–53 (1964).
2. S. Ostrach, Natural convection with combined driving forces, *PhysicoChem. Hydrodyn.* **1**, 233–247 (1980).
3. J. S. Turner, *Buoyancy Effects in Fluids*. Cambridge University Press, Cambridge (1973).
4. S. A. Thorpe, P. K. Hutt and R. Soulsby, The effect of horizontal gradients on thermohaline convection, *J. Fluid Mech.* **38**, 375–400 (1969).
5. C. F. Chen, D. G. Briggs and R. A. Wirtz, Stability of thermal convection in a salinity gradient due to lateral heating, *Int. J. Heat Mass Transfer* **14**, 57–65 (1971).
6. R. A. Wirtz, D. G. Briggs and C. F. Chen, Physical and numerical experiments on layered convection in a density stratified fluid, *Geophys. Fluid Dynam.* **3**, 265–288 (1972).
7. R. A. Wirtz and C. S. Reddy, Heat and mass transport across diffusive interfaces bounded by turbulent convecting regions, *Int. J. Heat Mass Transfer* **19**, 471–478 (1976).
8. L. W. Wang, Y. Kamotani and S. Ostrach, Experimental study of natural convection in a shallow horizontal cavity with different end temperatures and concentrations, FTAS/TR-82-164, Case Western Reserve University, Cleveland, Ohio (1983).
9. Y. Kamotani, L. W. Wang, S. Ostrach and H. D. Jiang, Experimental study of natural convection in shallow

enclosures with horizontal temperature and concentration gradients, *Int. J. Heat Mass Transfer* **28**, 165–173 (1985).
10. S. J. Khang and T. J. Fitzgerald, A new probe and circuit for measuring electrolyte conductivity, *Ind. Engng Chem. Fundam.* **14**, 208–213 (1975).
11. W. H. Kaufmann, *Sodium Chloride*. Reinhold, New York (1960).
12. A. Bejan, A. A. Al-Homoud and J. Imberger, Experimental study of high Rayleigh number convection in a horizontal cavity with different end temperatures, *J. Fluid Mech.* **109**, 283–299 (1981).

CONVECTION NATURELLE DANS DES FLUIDES CONFINES AVEC GRADIENTS DE TEMPERATURE ET DE CONCENTRATION HORIZONTALES

Résumé—La convection naturelle permanente d'une solution d'eau salée, due à des gradients de température et de concentration horizontales, est étudiée expérimentalement dans des enceintes rectangulaires de rapport de forme 0,2 et 2,0. Il apparait deux types de mouvement global de fluide : une configuration avec une seule cellule et une configuration multicouche, selon la valeur du rapport de flottement. On observe la formation et la croissance d'une structure stratifiée. Le nombre de couches qui apparaissent dans le cas des forces opposées d'origine thermique et solutale est plus grand que dans le cas des forces alliées. A cause de la nature diffusive de la chaleur et de la salinité, on obtient dans le régime multicouche des profils intéressants de température et de concentration.

NATÜRLICHE KONVEKTION IN EINGESCHLOSSENEN FLUIDEN MIT HORIZONTALEN TEMPERATUR- UND KONZENTRATIONSGRADIENTEN

Zusammenfassung—Die stationäre natürliche Konvektion einer Salzwasserlösung durch horizontale Temperatur- und Konzentrationsgradienten wurde in einem rechteckigen Behälter mit den Seitenverhältnissen 0,2 und 2,0 experimentell untersucht. Abhängig von der Größe des Auftriebsverhältnisses treten zwei verschiedene Bewegungen in der Flüssigkeit auf, eine zellulare Strömung und eine Mehrschichtenströmung. Die Entstehung und das Wachstum der geschichteten Strömung wurde beobachtet. Wirken die Auftriebskräfte aufgrund von Temperatur- und Konzentrationsunterschieden entgegengesetzt, dann entstehen mehr Schichten als wenn sie gleichsinnig wirken. Aufgrund der kombinierten Diffusionsprozesse von Wärme und Salz entstehen im Fall der Mehrschichtenströmung interessante Temperatur- und Konzentrationsprofile.

ЕСТЕСТВЕННАЯ КОНВЕКЦИЯ В ОГРАНИЧЕННЫХ ОБЪЕМАХ ЖИДКОСТИ ПРИ ОДНОВРЕМЕННОМ ВОЗДЕЙСТВИИ ГОРИЗОНТАЛЬНЫХ ГРАДИЕНТОВ ТЕМПЕРАТУРЫ И КОНЦЕНТРАЦИИ

Аннотация—В прямоугольных полостях с отношением сторон 0.2 и 2.0 экспериментально исследуется стационарная естественная конвекция водосолевого раствора, обусловленная одновременным воздействием горизонтальных градиентов температуры и концентрации. Обнаружено существование двух типов макроскопического движения жидкости, а именно, одноячейковая и многослойная структуры течения, в зависимости от относительной величины сил плавучести. Образование и рост многослойной структуры наблюдались визуально. Когда градиенты температуры и концентрации противоположны друг другу, возникает большее количество слоев, чем в случае, когда они совпадают по направлению. Благодаря одновременному действию тепловой и концентрационной конвекции получены своеобразные профили температуры и концентрации в режиме многослойного течения.